

## Journal Pre-proof

Eradicating intracellular MRSA via targeted delivery of Lysostaphin and Vancomycin with mannose-modified Exosomes

Xiaohong Yang, Beibei Xie, Haibo Peng, Gongming Shi, Banne Sreenivas, Jian Guo, Chenhui Wang, Yun He



PII: S0168-3659(20)30695-7

DOI: <https://doi.org/10.1016/j.jconrel.2020.11.045>

Reference: COREL 10678

To appear in: *Journal of Controlled Release*

Received date: 31 May 2020

Revised date: 17 October 2020

Accepted date: 23 November 2020

Please cite this article as: X. Yang, B. Xie, H. Peng, et al., Eradicating intracellular MRSA via targeted delivery of Lysostaphin and Vancomycin with mannose-modified Exosomes, *Journal of Controlled Release* (2020), <https://doi.org/10.1016/j.jconrel.2020.11.045>

This is a PDF file of an article that has undergone enhancements after acceptance, such as the addition of a cover page and metadata, and formatting for readability, but it is not yet the definitive version of record. This version will undergo additional copyediting, typesetting and review before it is published in its final form, but we are providing this version to give early visibility of the article. Please note that, during the production process, errors may be discovered which could affect the content, and all legal disclaimers that apply to the journal pertain.

© 2020 Published by Elsevier.

# Eradicating Intracellular MRSA via Targeted Delivery of Lysothaphin and Vancomycin with Mannose-modified Exosomes

Xiaohong Yang<sup>a,b,1</sup>, Beibei Xie<sup>b,1</sup>, Haibo Peng<sup>b,1</sup>, Gongming Shi<sup>b</sup>, Banne Sreenivas<sup>b</sup>, Jian Guo<sup>b</sup>, Chenhui Wang<sup>b\*</sup>, Yun He<sup>b\*</sup>

<sup>a</sup> Chongqing Institute of Green and Intelligent Technology, Chinese Academy of Sciences, 266 Fangzheng Ave, Shuitu Technology Development Zone, 400714 Beibei, Chongqing, China

<sup>b</sup> Chongqing Key Laboratory of Natural Product Synthesis and Drug Research, School of Pharmaceutical Sciences, Chongqing University, 55 Daxuecheng South Road, 401331 Shapingba, Chongqing, China

\* Corresponding author

E-mail address: Yun He, [yun.he@cqu.edu.cn](mailto:yun.he@cqu.edu.cn); Chenhui Wang, [wangchenhui@cqu.edu.cn](mailto:wangchenhui@cqu.edu.cn)

<sup>1</sup> Xiaohong Yang, Beibei Xie and Haibo Peng contributed equally to this work.

---

**ABSTRACT:** Intracellular methicillin-resistant *Staphylococcus aureus* (MRSA) is extremely difficult to remove by common antibiotics, leading to infection recurrence and resistance. Herein we report a novel exosome-based antibiotic delivery platform for eradicating intracellular MRSA, where mannose-decorated exosome (MExos) is employed as the drug carrier and preferentially taken up by macrophages, delivering lysothaphin (MExoL) and vancomycin (MExoV) to intracellular pathogens. Combination of MExoL and MExoV eradicated intracellular quiescent MRSA. Moreover, MExos rapidly accumulated in mouse liver and spleen, the target organs of intracellular MRSA, after intravenous (IV) administration. Thus, the MExos antibiotic delivery platform is a promising strategy for combating intracellular infection.

**Keywords:** Exosomes, Surface functionalization, Antibiotics, Targeted delivery, Intracellular infection

---

## 1. Introduction

The rising of bacterial resistance is a serious global public health problem <sup>1</sup>. There are more than 200,000 neonatal sepsis deaths with multidrug-resistant pathogens in low-income countries every year <sup>2</sup>. *Staphylococcus aureus* (*S. aureus*) is the main cause of bacterial infection in community settings and hospitals <sup>3</sup>. Methicillin-resistant *S. aureus* (MRSA) remains a formidable clinical threat, due to persistently high morbidity and mortality <sup>4</sup>. Macrophages are the first line of defense against bacterial infections by recognition, ingestion, and digestion of the invasive pathogens <sup>5</sup>. However, *S. aureus* can survive after ingestion by macrophages <sup>6</sup>. In this case, macrophages not only fail to eradicate bacteria but also serve as sources for bacterial propagation, leading to infection recurrence and resistance. More seriously, surviving bacteria in the host cells can protect themselves against the bactericidal action of antibiotics. In fact, most antibiotics are ineffective against intracellular pathogens due to their low retention inside the cells (i.e. macrolides or fluoroquinolones) <sup>7, 8</sup> or poor intracellular accumulation (i.e.  $\beta$ -lactams or aminoglycosides) <sup>9, 10</sup>. In particular, vancomycin is the last resort against MRSA but cannot eradicate intracellular MRSA due to its low uptake by infected host cells <sup>11</sup>. It is clear that despite considerable advances in antibiotic discovery, the treatment of intracellular bacterial infections remains a major challenge. Thus, targeted delivery of antibiotics to infected host cells especially macrophages is an important strategy to improve antibiotic therapy against intracellular infections.

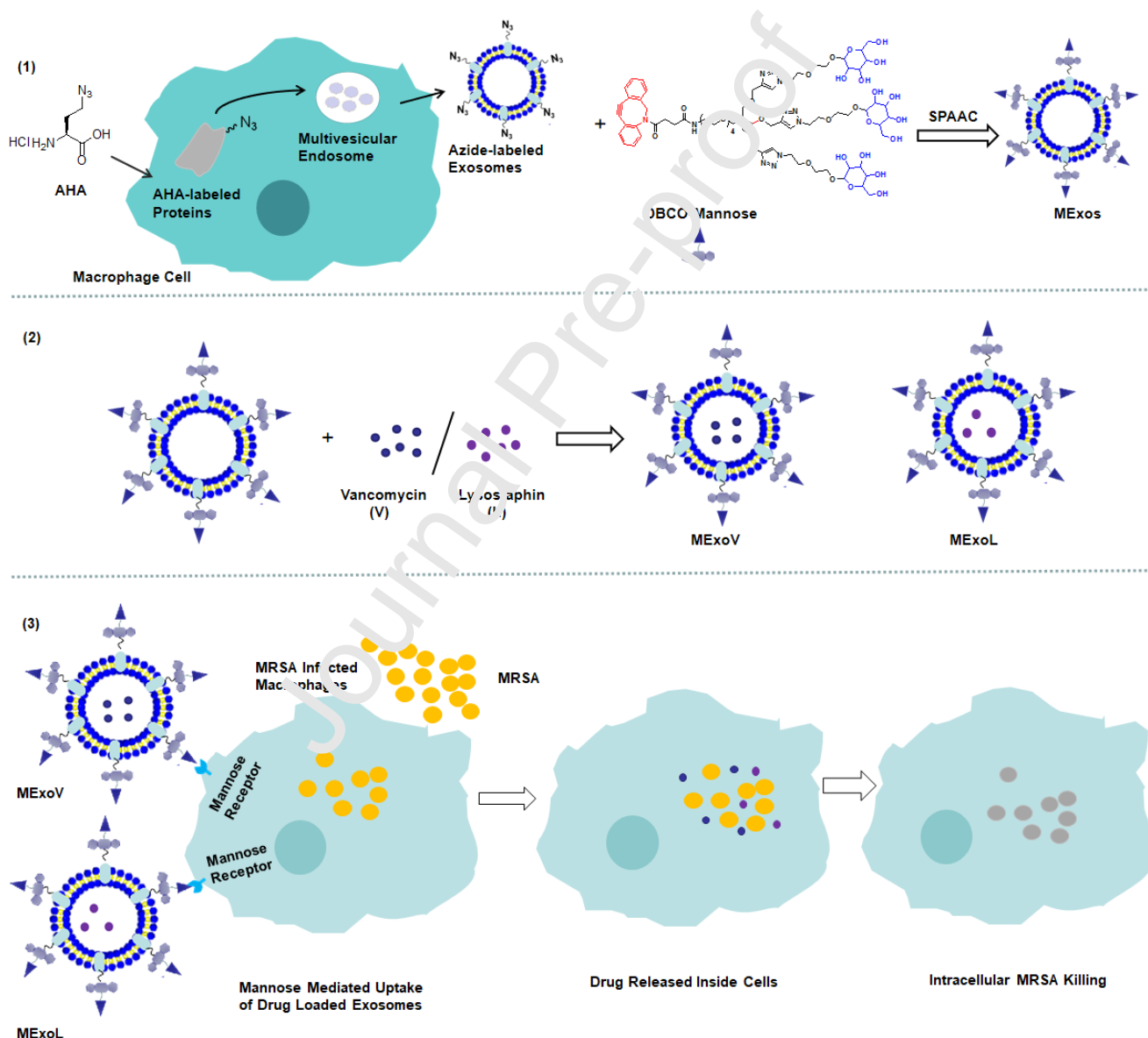


**Figure 1.** (1) Metabolic labeling of exosomes secreted by macrophages and bioorthogonal click conjugation for mannose-targeted exosomes (MExos); (2) Preparation of vancomycin (V) or lysostaphin (L) loaded mannose-targeted exosomes (MExoV or MExoL); (3) Eradication of intracellular MRSA by combination of MExoV and MExoL. SPAAC, strain-promoted azide-alkyne click chemistry reaction.

Intracellular *S. aureus* often present in a metabolically quiescent state <sup>12, 13</sup>, while most antibiotics including vancomycin are effective only against metabolically active bacteria. In this case, even increased intracellular uptake and accumulation of these antibiotics cannot

effectively eliminate intracellular bacteria. Lysostaphin is a 27-kDa antimicrobial enzyme and has antimicrobial activity specific against staphylococcal species *in vitro* and *in vivo*<sup>14-19</sup>. Importantly, there is accumulating evidence that lysostaphin kills not only planktonic bacteria but also quiescent bacteria growing in a biofilm<sup>20, 21</sup>. Lysostaphin is specifically able to cleave the cross-linking pentaglycine bides in the cell walls of *S. aureus*<sup>15</sup>, which makes its antimicrobial activity independent of the bacterial metabolic state. Therefore, it is potential to utilize the lysostaphin to kill intracellular quiescent bacteria if this enzyme is delivered into infected host cells. Moreover, combination of lysostaphin and vancomycin have synergistic antibacterial activity against extracellular *S. aureus* and MRSA<sup>22</sup>. It is presumed that if both lysostaphin and vancomycin are delivered into infected host cells, it would result in superior eradication of intracellular bacteria, decreased vancomycin treatment dose, reduced toxicity and resistance.

Exosomes have attracted considerable attention as drug delivery vehicles in the past few years<sup>23, 24</sup>. Exosomes are small intracellular membrane-based vesicles that are secreted by almost all kinds of cells<sup>25</sup>. Exosomes play crucial roles in intercellular communication and can efficiently deliver cargo to the recipient cells<sup>26, 27</sup>. Recently, exosomes, as drug delivery vehicles, have been used to treat various diseases, such as cancer<sup>28</sup>, cardiovascular diseases<sup>29</sup>, as well as Parkinson's and Alzheimer's disease<sup>30</sup>, and others. In our previous study, we discovered that exosomes could deliver antibiotic into cells and enhance intracellular MRSA killing without cytotoxicity<sup>31</sup>. Compared to other nanoparticle carriers like liposomes and polymeric nanoparticles, exosomes as drug carriers have many important advantages such as good biocompatibility, fewer side effects, long circulating half-life, and the intrinsic ability to target tissues<sup>32, 33</sup>.

Herein, we report a strategy for targeted antibiotic delivery to macrophages to treat intracellular MRSA infection, utilizing mannosylated exosomes as the drug carrier (Fig. 1). In this approach, azides are efficiently integrated into exosomes by altering the metabolic processes of exosome-secreting cells. DBCO-mannosyl ligands are conjugated to the azide-integrated exosomes by strain-promoted azide-alkyne click chemistry reaction (SPAAC), which would endow the exosomes with the advantages for targeted antibiotic delivery to macrophages that express high levels of the mannose receptor, as well as drug accumulation at bacterial infection sites through macrophage transport. Therefore, lysostaphin and vancomycin delivered to bacterial infection sites would exhibit enhanced eradication of intracellular bacteria.

## 2. Materials and Methods

### 2.1. Materials

Chemicals were used as received without special purification unless stated otherwise. <sup>1</sup>H and <sup>13</sup>C NMR spectra were recorded at ambient temperature on a 400 MHz NMR spectrometer (100 MHz for <sup>13</sup>C NMR). NMR results were reported in  $\delta$  units, parts per million (ppm), and were referenced to CDCl<sub>3</sub> (7.26 or 77.0 ppm) as the internal standard. The coupling constants *J* are given in Hz. Vancomycin (V) and lysostaphin (L) were purchased from Sango Biotech (Shanghai, China). CD63, tumor susceptibility gene 101 (TSG101) and Flotillin 1 antibodies were purchased from Abcam Biotechnology (Cambridge, MA, USA).  $\beta$ -actin and CD206 antibodies, and goat-anti-rabbit horseradish-peroxidase-conjugated (HRP) secondary antibody were purchased from Proteintech (Wuhan, China). The MRSA strain WHO-2 (WHO-2) was kindly provided by Rongxin Qin (Army Military Medical University, Chongqing, China). Female Balb/C and Kun Ming (KM) mice (aged 6-8 weeks) were purchased from Chongqing Byrness Weil Biotechnology Co.Ltd (Chongqing, China). L-Azidohomoalanine (AHA) was synthesized, purified and fully characterized as described previously<sup>34, 35</sup>.

### 2.2. Cell Culture

RAW264.7 cells were purchased from Shanghai Cell Bank of Chinese Academy of Sciences (Shanghai, China). Cells were cultured in high-glucose DMEM (Hyclone) medium supplemented with 10% fetal bovine serum (FBS), 1% penicillin and streptomycin at 37 °C in a 5% CO<sub>2</sub> humidified atmosphere. For AHA-integrated exosomes production, cells were maintained in conditioned medium composed of methionine- and cystine- depleted DMEM (Gibco, Grand Island, NY, USA) with 10% exosome-free FBS in the presence of AHA (100, 200, 300 and 400  $\mu$ M) as previously described<sup>36</sup> with minor modifications<sup>36</sup>. FBS were centrifuged at 120,000  $\times$  g for 140 min to remove serum exosomes.

### 2.3. Isolation of Exosomes

Exosomes were purified as previously described<sup>36, 37</sup> with minor modifications. Briefly, cells were cultured with conditioned medium for 48 h. The cell culture supernatant containing exosomes were centrifuged at 200  $\times$  g for 5 min, to remove cells, and then centrifuged at 12,000  $\times$  g for 30 min, to eliminate dead cells and cell debris. The resulting supernatant was ultrafiltered through a 100 kDa membrane to concentrate the exosome-containing solution, which was used to isolate exosomes by ultracentrifugation at 100,000  $\times$  g (Beckman Corp, Brea, CA, USA) for 90 min. The pellet was washed with PBS and centrifuged at 120,000  $\times$  g for 120 min. Finally, exosomes were resuspended in PBS and stored at -80 °C prior to use. All procedures were carried out at 4 °C. The exosome protein concentration was measured by BCA kit (Beyotime, China).

### 2.4. Characterization of Exosomes

Particle size and morphology were characterized according to our previous study<sup>31</sup>. The particle size distribution and zeta potential of exosomes in suspension were measured using a multi angle particle size and high sensitive zeta potential analyzer (Brookhaven NanoBrook Omni, Brookhaven, USA). A transmission electron microscope (TEM; HT7700, Hitachi, Japan) was used to observe the morphology of exosomes.

Protein levels in exosomes (CD63, TSG101 and Flotillin 1) were analyzed by western blotting as previously described<sup>31, 38</sup>. Exosomes solution was denaturized with sodium dodecyl sulfate-polyacrylamide electrophoresis gels (SDS-PAGE) loading buffer at 100 °C for 10 min. The exosomal proteins were separated by 12% SDS-PAGE and were then transferred onto polyvinylidene fluoride (PVDF) membranes. Subsequently, the PVDF were blocked in tris-buffered saline with 5% fat-free dry milk at room temperature for 2 h,

breezed with desired antibodies including CD63, TSG101, Flotillin 1 and  $\beta$ -actin overnight, and then incubated with secondary antibodies. Finally, the resolved bands were visualized by enhanced chemiluminescence (ECL)-detecting reagents (Beyotime, Jiangsu, China) on a ChemiDoc system (BioRad, Shanghai, China).

## 2.5. Conjugation of DBCO-RohB with AHA-exosomes

AHA-metabolized exosomes at concentration of 5 mg/mL of protein were incubated with DMSO solution of DBCO-RohB (10  $\mu$ M final concentration) for 3 h at room temperature, followed by purification using MW 3000 Exosome Spin Columns (Thermo Fisher Scientific, Shanghai, China). The concentration of exosome was quantified by BCA protein assay, the RohB concentration was determined by measuring the absorbance of RohB using a SpectraMax® i3x microplate reader (SpectraMax i3x, Molecular Device, UK) and normalizing exosome protein concentration to 1 mg/mL. As a comparison, exosomes secreted from RAW264.7 cells without AHA pre-treatments were mixed with DBCO-RohB similarly.

## 2.6. Intracellular Delivery of AHA-RohB Conjugated Exosomes

RAW264.7 cells were seeded on coverslips in 24-well plates ( $2 \times 10^4$  cells/well) overnight and then were incubated with AHA-RohB exosomes (with 100 nM of RohB) for 3 h. Cells were washed three times with PBS solution and then fixed with 4% paraformaldehyde (PFA) for 20 min. Subsequently, cells were washed twice with PBS solution. Finally, cells were viewed under a confocal laser scanning microscopy (CLSM; Leica TCS SP8, Solms, Germany). Free DBCO-RohB or a mixture with exosome secreted by untreated RAW264.7 cells were similarly exposed to RAW264.7 cells as negative controls.

## 2.7. DBCO-mannose Conjugation

For mannose-exosomes, AHA-metabolized exosomes (5 mg/mL of protein) were incubated with DBCO-mannose (250  $\mu$ M of final concentration) for 2 h at room temperature, followed by purification using MW 3000 Exosome Spin Columns (Thermo Fisher Scientific, Shanghai, China). The mannose-conjugated exosomes (mannosylated exosome) were dispersed in PBS and stored at -80 °C before use.

## 2.8. Fluorescence Labeled Exosomes

The lipophilic fluorescent dyes 3, 3'-di-octadecyloxarocyanine perchlorate (DiO) and 1,1'-di-octadecyl-3,3',3'-tetramethylindodicarbocyanine,4 chlorobenzenesulfonate salt (DiD) (Beyotime, Jiangsu, China) were used to label lipid membrane of exosomes. Purified exosomes were incubated with 30  $\mu$ M of DiO or DiD for 15 min at 37 °C, then the extra dye was removed by MW 3000 Exosome Spin Columns. Labeled exosomes were then quantitated by determining the fluorescence intensity at an excitation wavelength of 484 nm and an emission wavelength of 501 nm. The labeled exosomes were resuspended in PBS prior to use.

## 2.9. Uptake of DiO-labeled Mannosylated Exosomes in Cells

For flow cytometry analysis, RAW264.7 cells or A549 cells were grown in 24-well plates at a density of  $5 \times 10^4$  cells per well and incubated with DiO labeled exosomes or mannosylated exosomes (100  $\mu$ g/mL) for 3 h. In the competitive inhibition assay, cells were incubated with D-mannosamine hydrochloride at a final concentration of 50 mM for 1 h before the addition of exosomes. Finally, cells were collected, washed three times with PBS, resuspended in 200  $\mu$ L of PBS and subjected to flow cytometric analysis. For microscopic observation, RAW264.7 cells ( $2 \times 10^4$  cells/well) were seeded on coverslips in 24-well plates overnight. Cells were treated as described above in the flow cytometry analysis section. At the end of uptake, cells were washed three times with PBS solution and fixed with 4% PFA for 20 min. Then the nuclei were stained with 4', 6-diamidino-2-phenylindole (DAPI; Beyotime, Jiangsu, China) and viewed with a CLSM (Leica TCS SP8, Solms, Germany).

## 2.10. Preparation of Vancomycin-loaded Mannosylated Exosomes (MExoV)

The vancomycin loaded exosomes were prepared with minor modifications as previously described<sup>30</sup>. To load the exosomes with vancomycin, 100  $\mu$ g of purified exosomes were mixed with 50  $\mu$ g of vancomycin. The vancomycin-exosome mixture was sonicated using a Model 505 Sonic Dismembrator with 25"tip with the following settings: 20% power, 10 cycles of 4s pulse/2s pause. After 5 cycles, exosomes were cooled down for 2 min on ice, and then the other 5 cycles were performed. After sonication, the vancomycin-exosome mixture was incubated at 37 °C for 60 min to allow for recovery of the exosomal membrane. Recovery was assessed by DLS and TEM as described above (2.4). Excess free drug was separated from vancomycin-exosome mixture by ultrafiltration purification using Amicon1 Ultra Centrifugal Filters (MWCO = 100 kDa, GE Healthcare, UK). The Exodrug mixture was filtered using a 0.22  $\mu$ m syringe filter (Millipore, Billerica, MA) for sterility, and stored at -80 °C until use.

The exosomes loaded with vancomycin (MExoV or ExoV) were quantified for the encapsulated vancomycin by a high performance liquid chromatography (HPLC) method as previously reported<sup>31,39</sup>, with minor modification. Specifically, appropriate volume of acetonitrile (ACN) was mixed fully with MExoV or ExoV solution in a micro-centrifuge tube. After sonication, the mixture was centrifuged at  $18,000 \times g$  for 10 min. Subsequently, the supernatant was taken and filtered through a syringe filter (0.2  $\mu$ m) and transferred into HPLC autosampler vials. 20  $\mu$ L of aliquot was injected into the HPLC system (Agilent 1260, Agilent Technologies, Palo Alto, CA). All analyses were performed using a C18 column (Extend-C18, 250 mm  $\times$  4.6 mm, 5  $\mu$ m, 100 Å, Agilent) with a mobile phase of KH<sub>2</sub>PO<sub>4</sub>: ACN (90:10; v/v; pH = 3.2) at a flow rate of 1 mL/min at 30 °C. Absorbance was measured at 236 nm to monitor the elution of vancomycin. The standard curve for vancomycin was obtained from 0.5 to 100  $\mu$ g/mL concentration range. For data acquisition and analysis, OpenLAB CDS ChemStation Edition software was used.

## 2.11. Preparation of Lysostaphin-loaded Mannosylated Exosomes (MExoL)

Lysostaphin loaded exosomes were prepared as described above for MExoV, with a slight modification for sonication. The lysostaphin-exosome mixture was sonicated with the following settings: 30% power, 12 cycles of 4s pulse/2s pause. After 6 cycles, exosomes were cooled down for 2 min on ice, and the other 6 cycles were then performed. Excess free lysostaphin was also removed by ultrafiltration using Vivaspin500 (MWCO=100 KDa, GE Healthcare, UK). To determine drug loading efficiency, the concentration of lysostaphin in filter liquor was determined by BCA method.

### 2.12. *In vitro* Release of Vancomycin

The *in vitro* release profile of vancomycin was determined in four different media as previously described<sup>31</sup>. The media included 1) PBS at pH 7.4, 2) sodium citrate 0.1 M citrated PBS (CPBS) at pH 4.5, 3) PBS at pH 7.4 with 1 mg of RAW264.7 cell lysates, and 4) CPBS at pH 4.5 with 1 mg of RAW264.7 cell lysates. Freshly prepared MExoV was placed in a dialysis bag (MW = 100K). Then the dialysis bag was placed in the above mentioned media, which were incubated with continuous shaking at 80 rpm in a shaker bath (WE-1 Shaking water bath; Tianjin Honor Inc.) at 37 °C. At desired time point, 200 µL aliquots of the samples were collected and analyzed by HPLC.

### 2.13. Intracellular Accumulation of Vancomycin in Macrophages

RAW264.7 cells were seeded in 24-well plates ( $5 \times 10^4$  cells/well) and infected by MRSA as described above for the determination of intracellular MRSA survival. After that, cells were incubated with V, ExoV or MExoV (100 µg/mL equiv. V) for 4 h. After incubation, cells were collected after thorough washing with pre-warmed PBS and lysed by adding ACN at a final concentration of 75% (v/v). Then, the antibiotic accumulation in cell lysates was determined by HPLC.

### 2.14. Intracellular MRSA Infection Model

For both RAW264.7 macrophages and A549 cells, infection by MRSA WHO-2 was performed with minor modifications as previously described<sup>31, 40</sup>. Cells were seeded in 24-well plates ( $5 \times 10^4$  cells/well) and incubated overnight. MRSA were then added to the cell culture medium of either RAW264.7 macrophages or A549 cells at a ratio of 10–20 bacteria per cell and maintained for 2 h (2 h infection model) or 24 h (24 h infection model) at 37 °C. Extracellular bacteria were killed by adding gentamicin (50 µg/mL).

### 2.15. Effects of MExoV and MExoL on the Growth of Intracellular MRSA in 2 h Infected Macrophages and A549 Cells

Infected cells (2 h infection model) were incubated with free vancomycin, lysostaphin, or their exosome formulations. After 24 h treatment, the medium was removed, and cells were quickly washed twice with PBS. Then cells were lysed with Hanks buffered saline solution (HBSS) supplemented with 0.1% bovine serum albumin (BSA) and 0.1% Triton-X, and serial dilutions of the lysate were made in PBS solution containing 0.05% Tween-20. The number of surviving intracellular bacteria was determined by plating on tryptic soy agar plates with 5% defibrinated sheep blood.

### 2.16. MIC Determination for Free Antibiotics on Extracellular Planktonic Bacteria.

Minimal inhibitory concentration (MIC) of vancomycin or lysostaphin against extracellular MRSA WHO-2 was determined using planktonic bacteria as previously described<sup>41</sup>. Dilutions of drugs were made in the 96-well culture plate. Bacteria were cultured in Mueller-Hinton broth II medium (Solarbio, Beijing, China).  $5 \times 10^4$  colony forming units (CFU) of MRSA suspension from an exponentially growing culture were added into the plate with drug mentioned above. After incubation at 37 °C for 20 h, bacterial growth was monitored by reading the optical density (OD) at 600 nm. The concentration that inhibited bacterial growth by more than 90% was considered as the MIC of antibiotic.

### 2.17. Time of Kill for Free Antibiotics on Non-replicating Bacteria

Killing of non-replicating MRSA by free vancomycin or lysostaphin was determined as previously described<sup>40</sup>. Briefly, MRSA WHO-2, from an overnight stationary phase culture, were incubated with or without antibiotics for 24 h. At each desired time, bacteria were collected and then cultured on agar plates to detect the CFU of surviving bacteria.

### 2.18. Effects of Combination of MExoV and MExoL on the Growth of Intracellular MRSA in 2 h and 24 h Infected Macrophages

After infection with MRSA for 2 h or 24 h, RAW264.7 cells were incubated with combination of MExoV and MExoL for 24 h. MExoV or MExoL alone treatment was used as the control study. After drug treatment, intracellular survival CFU of MRSA was accessed as described above (2.15) for the assessment of drug loaded exosomes against intracellular MRSA. For microscopic observations, cells were infected by MRSA and treated with drug as described above for CFU determination. After 24 h treatment, cells were washed by PBS, fixed with 4% PFA, and permeabilized with 0.2% Triton-X100 for 5 min. Then, cells were incubated with the mixture of the LIVE/DEAD BacLight bacterial viability kit for 15 min in the dark. After washing with PBS, cells were observed using a CLSM (Leica TCS SP8, Solms, Germany).

### 2.19. Antibacterial Effects of MExoV and MExoL in MRSA-Infected Mice

Mice were housed at 21 °C ± 1 °C with a 12-hour light/12-hour dark cycle. All animals had free access to food and water throughout the experiment. All animal studies were approved by the Laboratory Animal Welfare and Ethics Committee of the Third Military Medical University, and the animal handling procedures followed the guidelines set by the Animal Care Committee, Third Military Medical University.

To test the antibacterial effect *in vivo*, bacteria-infected mouse model were carried out by intraperitoneal injection of MRSA ( $5 \times 10^7$  CFU) with minor modifications as previously described<sup>31, 42</sup>. After 24 h of infection (day 1), mice were randomly assigned into 6 treatment

groups (5 mice/group), including PBS, Vancomycin (V; 20 mg/kg), Lysostaphin (L; 5 mg/kg), MExoV (V = 20 mg/kg), MExoL (L = 5 mg/kg), MExoV and MExoL (V = 20 mg/kg; L = 5 mg/kg).

For testing efficacy in mouse peritoneum, each drug was injected intravenously at a single dose for 24 h. After treatment, mice were sacrificed and injected with 3 mL HBSS intraperitoneally. Then, peritoneal fluid was collected from the peritoneum, which was used to determine the total CFU count, extracellular count and intracellular count: (1) The total CFU in the peritoneal fluid was quantified before any further procedures were carried out; (2) Separation of extracellular and intracellular bacteria in the peritoneal fluid: the peritoneal fluid was equally divided into fractions A (extracellular CFU quantification) and fractions B (intracellular CFU quantification). For extracellular CFU count, fraction A was centrifuged at 300 × g for 10 min at 4 °C and the bacteria in the supernatant was quantified. For intracellular CFU count, fraction B was incubated with 15 µg/mL of lysostaphin (Sangon Biotech, Shanghai, China) for 20 min at room temperature. Subsequently, the lysostaphin was removed by washing three times with PBS. Finally, the samples were incubated with HBSS (0.1% BSA and 0.1% Triton-X) for 10 min and the intracellular CFU was quantified by tryptic soy agar plates.

For testing efficacy in kidney, each drug was administered intravenously once a day for 3 days. On day 4 after infection, all mice were sacrificed and kidneys were harvested in 1 mL of PBS. The tissue samples were homogenized with a high-throughput tissue homogenizer (Sceintz-48, Ningbo, China). The survival bacteria recovered per mouse (two kidneys) were measured by tryptic soy agar plates.

## 2.20. Acute Toxicity of MExos and MExodrug in Mice

Female Balb/C mice (aged 6-8 weeks) were treated with MExos (2.5 mg/kg), MExoV (V=100 mg/kg) or MExoL (L=25 mg/kg) by intravenous injection. The control group was injected with PBS. Drugs were administered intravenously once a day for 3 days. On day 4 after the first injection, all mice were sacrificed by intraperitoneal injection of pentobarbital sodium (1%). Then, the major organs (heart, liver, spleen, lung and kidney) were harvested, formalin-fixed, subjected to Hematoxylin and Eosin (H&E) staining for evaluating histological morphology.

## 2.21. Localization of MExos in MRSA Infected RAW264.7 Cells

RAW 264.7 cells were infected with MRSA for 24 h in 24-well chamber slides and were then incubated with DiO labeled MExos for 24 h. Subsequently, cells were washed two times with PBS solution and then incubated with 100 nM of Lyso-Tracker Red (Beyotime, Jiangsu, China) for 30 min. After that, cells were washed with PBS three times and fixed with 4% PFA for 20 min. Finally, cells were observed using a CLSM (Leica TCS SP8, Solms, Germany).

## 2.22. In vivo Biodistribution of MExos in Mice

To study the biodistribution of exosomes, DiD-labeled MExos were injected into tail veins of KM mice. Then, the *ex vivo* images were visualized from sacrificed mice using an IVIS imaging system. (PerkinElmer).

**Table 1.** Physicochemical characteristics of exosomes and drug loaded exosomes

Formulation	Size (nm)	PDI	Zeta Potential (mV)	Loading Capacity (%)
Exos	96.39 ± 5.85	0.265 ± 0.004	-6.96 ± 1.25	N
AHA-RohB Exos	93.10 ± 10.13	0.243 ± 0.004	-7.25 ± 1.38	N
MExos	100.25 ± 10.00	0.251 ± 0.005	-10.85 ± 2.31	N
MExos, sonicated	146.86 ± 10.76	0.253 ± 0.010	-9.13 ± 1.82	N
MExoV	150.22 ± 13.77	0.240 ± 0.010	-8.22 ± 1.54	22.15 ± 3.21
MExoL	152.25 ± 10.12	0.260 ± 0.020	-9.58 ± 2.05	15.52 ± 2.38

Note: Data is presented as mean ± SD.

Abbreviations: Exos, AHA-metabolized exosomes; AHA-RohB Exos, DBCO-RohB conjugated AHA-metabolized exosomes; MExos, mannosylated exosomes; MExoV, V loaded mannosylated exosomes; MExoL, L loaded mannosylated exosomes; V, vancomycin; L, lysostaphin.

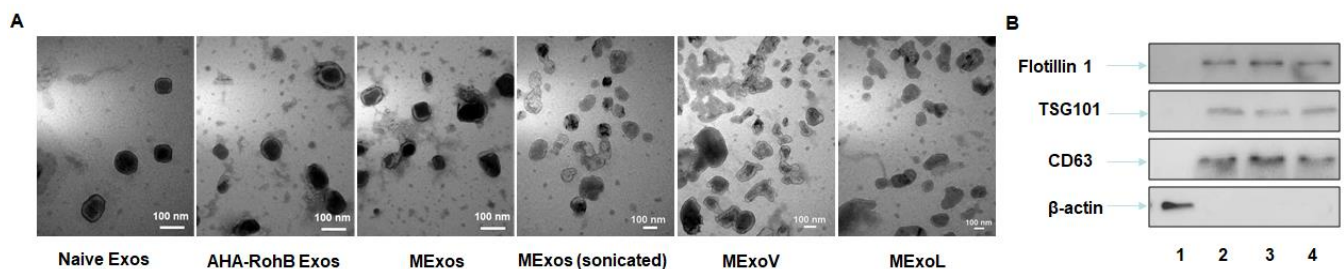


**Figure 2.** Characterization of unmodified and modified exosome formulations. Vancomycin or lysostaphin was incorporated into exosomes by sonication. (A) The morphology of drug-loaded exosomes was examined by TEM. (B) Western blot data indicated that formulations retained the exosome markers CD63, TSG101 and flotillin 1 after the copper-free click chemistry and the sonication procedure. 1, cell lysis; 2, Exos; 3, AHA-RohB Exos; 4, MExoV.

### 2.23. Statistical Analysis

For the all experiments, data were expressed as the mean  $\pm$  standard deviation (SD). Data analysis was performed by using the SPSS (V19.0, SPSS Inc., Chicago, IL, USA). Tests for significant differences between the groups were performed using student's t-test or one-way ANOVA.  $P < 0.05$  was considered statistically significant.

## 3. Results and Discussion

### 3.1. Preparation, Purification, and Characterization of AHA-exosomes

The metabolized exosomes were obtained by co-culturing AHA with exosome-secreting RAW264.7 cells for three days and then isolating exosomes using differential ultracentrifugation. The size distribution and zeta potential of AHA-metabolized exosomes were determined by dynamic light scattering (DLS) analysis. As shown in **Tab. 1**, their average diameters were  $96.39 \pm 5.85$  nm with a relatively low polydispersity, and they were negatively charged (zeta potential =  $-6.96 \pm 1.25$  mV) in PBS. The TEM images revealed that the isolated exosomes had a round morphology (**Fig. 2A**). Moreover, exosomal markers were detected by western blotting and exosomes were enriched with CD63, Flotillin 1 and TSG101 (**Fig. 2B**). These data showed that exosomes were successfully purified.

To confirm the successful incorporation of AHA into exosomes during the cell co-culture process, DBCO-RohB was synthesized by the methods shown in **Fig. 3**. AHA-metabolized exosomes were incubated with fluorescent DBCO-RohB and the RohB conjugation efficiency was determined after removing the excess DBCO-RohB from the reaction mixtures. As shown in **Fig. 4A**, compared to the control exosomes, AHA-exosomes showed strong and increasing fluorescent intensity with increasing AHA concentrations, suggesting efficient click conjugation between AHA-metabolized exosomes and DBCO-RohB. Additionally, after DBCO-RohB clicking, the size and shape were not significantly changed (**Tab. 1** and **Fig. 2A**). And

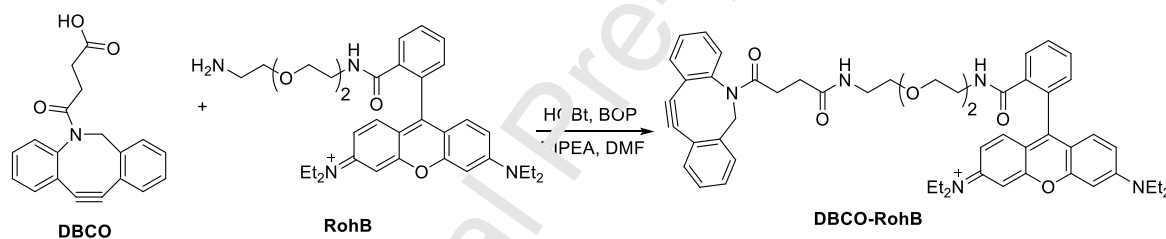


**Figure 3.** Synthetic route to DBCO-RohB

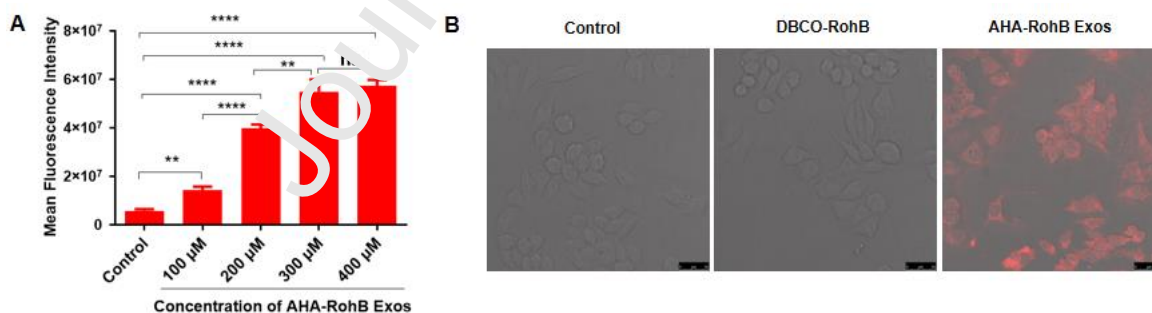


**Figure 4.** (A) The mean fluorescence intensity of RohB in the DBCO-RohB conjugation of exosomes. DBCO-RohB was incubated with AHA- exosomes (AHA = 100 - 400  $\mu$ M) or the control exosomes. After conjugation, the RohB absorption was measured by a SpectraMax® i3x microplate reader and exosome protein concentration was normalized to 1 mg/mL. (B) CLSM images of RAW264.7 cells treated with i) DBCO-RohB mixed with unmodified exosomes, ii) Free DBCO-RohB, iii) AHA-RohB exosomes for 3 h. Scale bars: 25  $\mu$ m. \*,  $p < 0.05$ ; \*\*,  $p < 0.01$ ; \*\*\*,  $p < 0.001$ ; \*\*\*\*,  $p < 0.0001$ .

the significant difference in exosome surface marker protein levels (CD63, Flotillin 1 and TSG101) was not observed between the control exosomes and AHA-exosomes (**Fig. 2B**). Taken together, these data showed that azides were efficiently integrated into exosomes and the conjugation had no impact on the exosome structure and function. The azide-integrated exosomes provide a convenient approach for functionalizing the exosome surface by SPAAC conjugation.

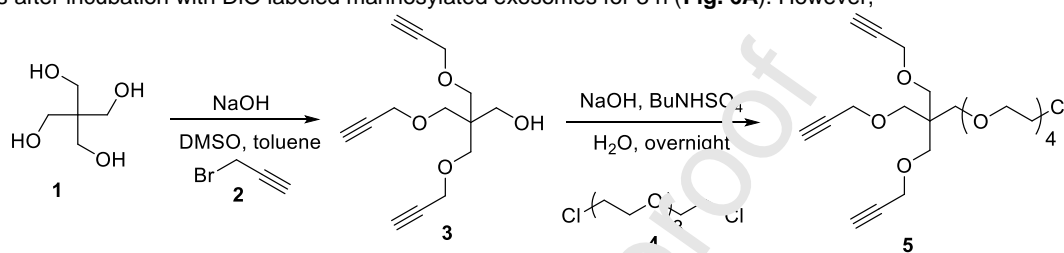
In order to further investigate whether the modified exosomes could efficiently transport cargo into cells, RAW264.7 cells were incubated with AHA-RohB conjugated exosomes and visualized by CLSM. As shown in **Fig. 4B**, treatment of RAW264.7 cells with AHA-RohB conjugated exosomes resulted in significant RohB accumulation in the cytosol, whereas no obvious RohB fluorescent signal was observed in cells treated with a mixture of DBCO-RohB and unmodified exosomes, and free DBCO-RohB. These results suggested that AHA-integrated exosomes could conjugate with DBCO-cargo and efficiently deliver them into cells. Thus, surface functionalized exosomes could serve as a novel nanocarrier for targeted drug delivery.

### 3.2. Preparation and Characterization of Mannosylated Exosomes

DBCO-mannose was synthesized and the synthetic route is illustrated in **Fig. 5**. To obtain mannosylated exosomes (MExos), DBCO-mannose was reacted with azide-integrated exosomes to form stable triazole linkages using copper-free click chemistry. The size distribution, zeta potential and morphology of mannosylated exosomes were also similar to that of unmodified exosomes (**Tab. 1**, **Fig. 2A and B**), suggesting DBCO-mannose conjugation did not alter the structure and function of exosomes.

### 3.3. Cell Uptake of Mannosylated Exosomes.

To demonstrate that mannosylated exosomes could indeed facilitate entry into macrophages, mannosylated exosomes and unmodified exosomes were labeled with lipophilic dye DiO. These DiO labeled exosomes were incubated with RAW264.7 cells and A549 cells, respectively. The DiO fluorescence of cells was analyzed by FACS and CLSM. RAW 264.7 cell is a mouse macrophage cell line, expressing high levels of mannose receptor on the cell surface, whereas A549 cell is a human bronchial epithelial cell line with no expression of this receptor. According to the flow cytometric analyses, the strongest fluorescence was measured in macrophages after incubation with DiO labeled mannosylated exosomes for 3 h (**Fig. 6A**). However,



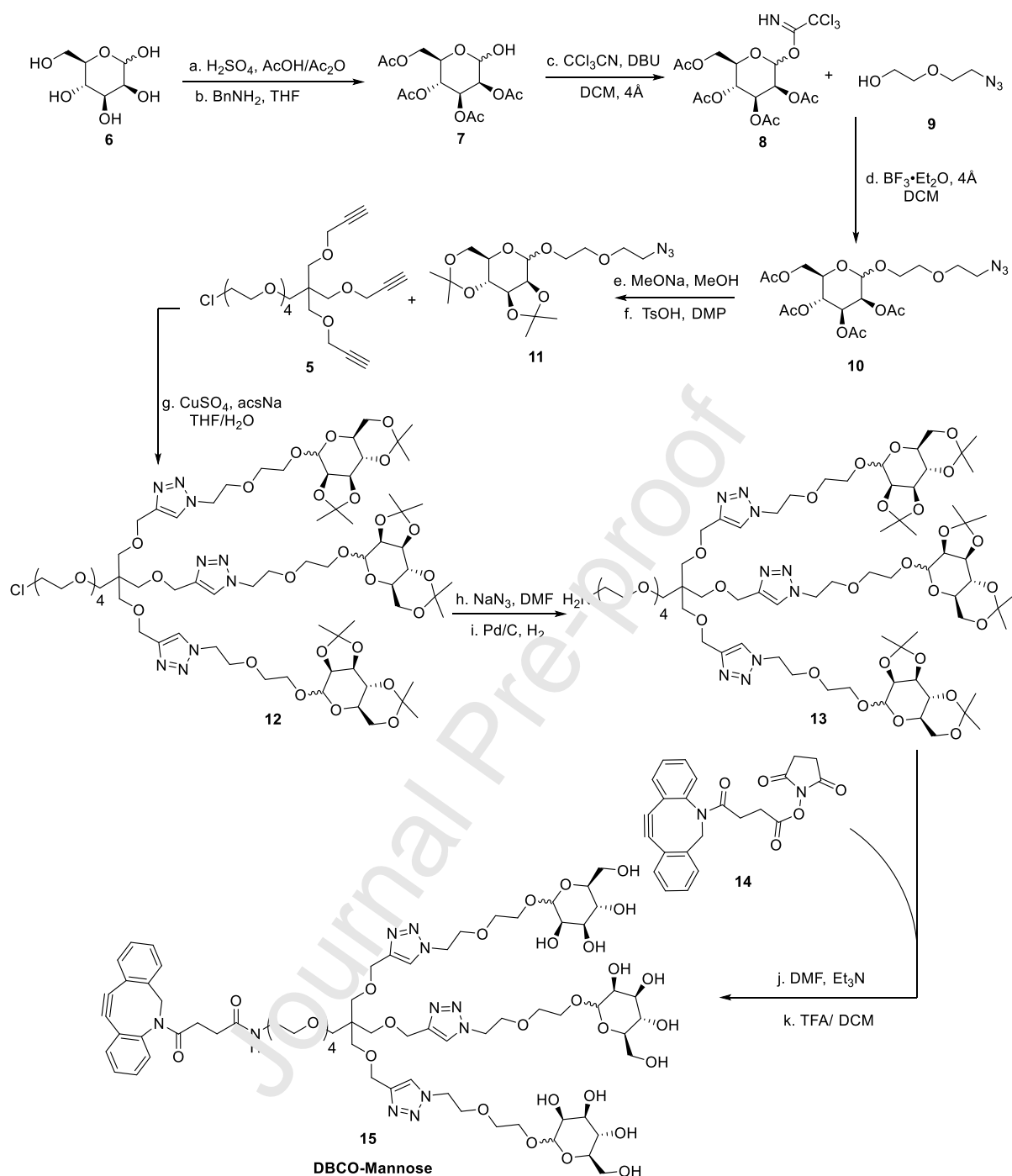
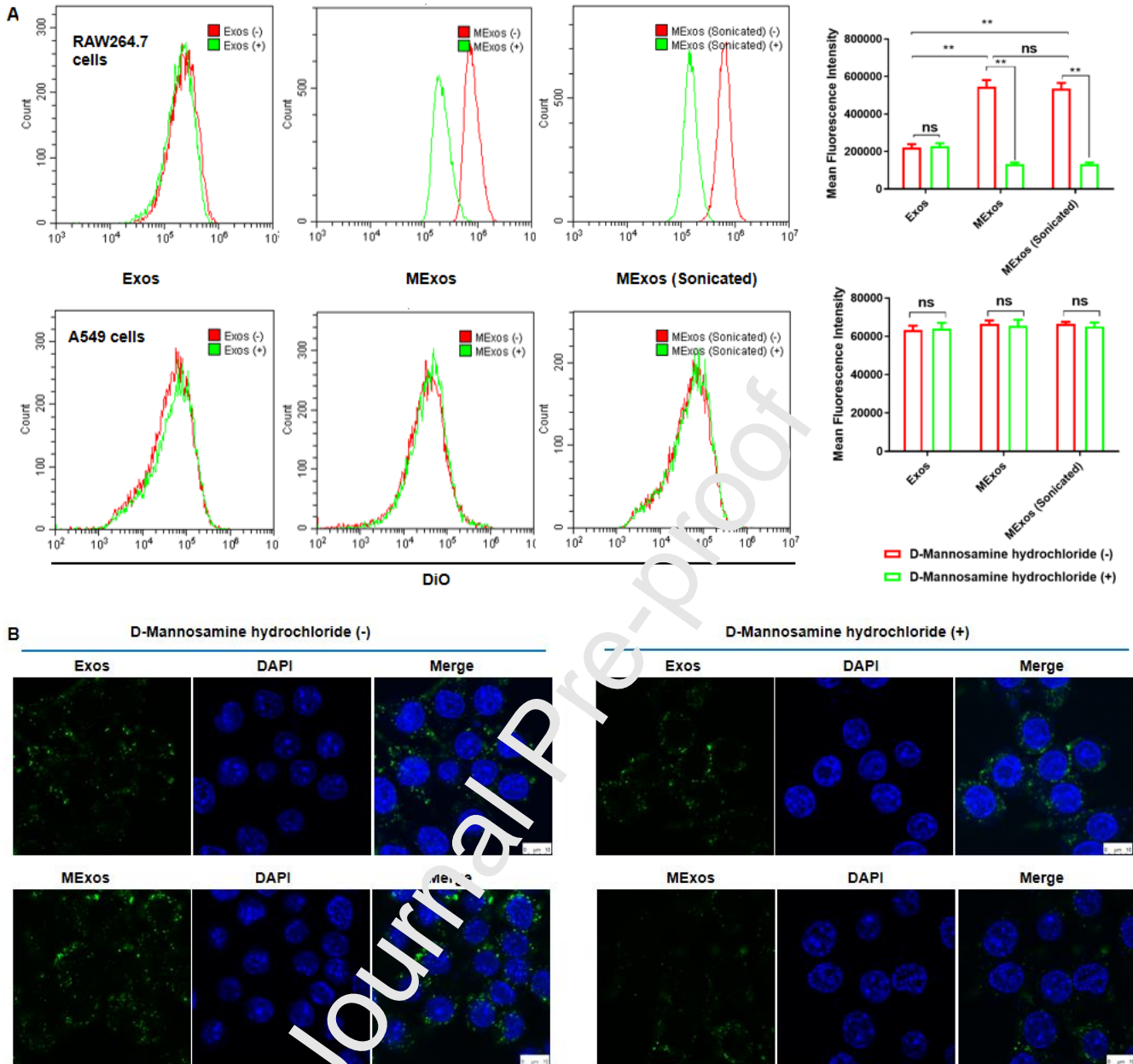


Figure 5. Synthetic route of DBCO-Mannose

pretreatment of macrophages with D-mannosamine (a known mannosamine inhibitor) significantly decreased intracellular fluorescence level, while this phenomenon was not observed in A549 cells, suggesting that the mannosamine inhibitor competitively prevented entry of mannosylated exosomes into macrophages. CLSM images also showed that treatment of macrophages with mannosylated exosomes exhibited higher fluorescence intensity of DiO than that of unmodified exosomes at the same exosome concentration (Fig. 6B). This suggests that a specific interaction between mannosylated exosomes and the cell surface might occur.



**Figure 6.** Uptake of Exos and MEXos by RAW264.7 cells and A549 cells. The mean fluorescence intensity of cells was determined by flow cytometric analyses after incubation with DiO labeled Exos, MEXos or MEXos (sonicated) at the same dose of exosomes (A). The photos were taken with confocal microscopy (B). In the competitive inhibition assay, cells were incubated with D-mannosamine hydrochloride at a final concentration of 50 mM for 1 h before the addition of exosomes. Scale bars: 10  $\mu$ m. Exos, exosomes; MEXos, mannoseylated exosomes. \*,  $p < 0.05$ ; \*\*,  $p < 0.01$ .

### 3.4. Manufacture and Characterization of Drug Loaded Mannosylated Exosomes

Vancomycin and lysostaphin exhibit poor intracellular penetration into cells, and both of them are unable to eradicate intracellular MRSA, although they have good extracellular antibacterial effect. To test the potential of the mannoseylated exosomes as a carrier for these antibacterial drugs, vancomycin (V) or lysostaphin (L) was incorporated into mannoseylated exosomes by mild sonication and their loading efficiency (MExoV and MExoL) were  $22.15\% \pm 3.21\%$  and  $15.52\% \pm 2.38\%$ , respectively (Tab. 1). DLS studies revealed that the size of MExodrug nanoformulations increased similarly (Tab. 1) and exosomes sonicated in the absence of drug were even larger than the naive exosomes, but the zeta potential of these all nanocarriers were not significantly altered. In addition, retention of shape and round morphology of exosomes (Fig. 2A) were observed under TEM. Interestingly, MExoV were also enriched with exosomal markers (CD63, TSG101 and Flotillin 1) (Fig. 2B). These data suggested that there was no major alteration of the lipid content of exosomal membrane and its membrane microviscosity was completely restored after sonication.

### 3.5. In Vitro Release of MExoV

We next determined the *in vitro* release profiles of vancomycin in four different media (buffer solution at pH 4.5 and 7.4 with or without cell lysates). As shown in Fig. 7A, MExoV showed burst release within the first four hours in media with cell lysates, and thereafter displayed a sustained release profile thereafter. Specifically,  $18.79 \pm 1.53\%$  and  $18.53 \pm 2.52\%$  of the total encapsulated vancomycin were released from exosomes in 1 h for media with cell lysates at pH 4.5 and 7.4, respectively, and reached  $68.92 \pm$

5.03% and  $64.35 \pm 4.04\%$  in 4 h, respectively. When not incubated with cell lysates, the cumulative drug release reached  $66.02 \pm 2.52$  and  $70.7 \pm 1.0\%$  in 8 h at pH 4.5 and 7.4, respectively, which was lower than that for media with cell lysates ( $85.49 \pm 2.65$  and  $79.48 \pm 0.58\%$ , respectively). Moreover, the release kinetics was similar in CPBS (pH 4.5) and PBS (pH 7.4), suggesting a minimal effect of pH. It is worth noting that cell lysates promoted the cumulative release of vancomycin from exosomes.

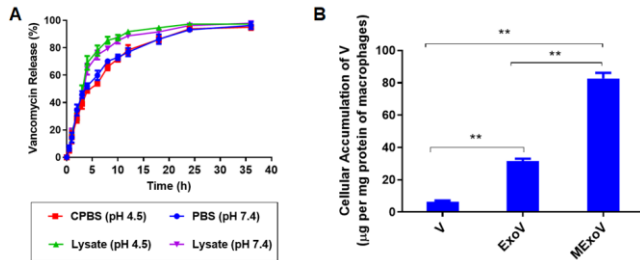


**Figure 7.** *In vitro* release and cellular accumulation of vancomycin in exosome formulations. (A) *In vitro* release of V from MExoV in four types of media. MExoV was incubated at pH 4.5 or 7.4 in the presence or absence of cell lysates at 37 °C and V release was estimated by HPLC. Data represent the mean  $\pm$  SD of three independent experiments in triplicate. (B) Cellular accumulation of V in RAW264.7 cells. After incubation with free V, ExoV or MExoV (V = 100 µg/mL) for 4 h, intracellular V was determined by HPLC method. V, vancomycin; ExoV, vancomycin loaded exosomes; MExoV, vancomycin loaded mannoseylated exosomes. \*,  $p < 0.05$ ; \*\*,  $p < 0.01$ .

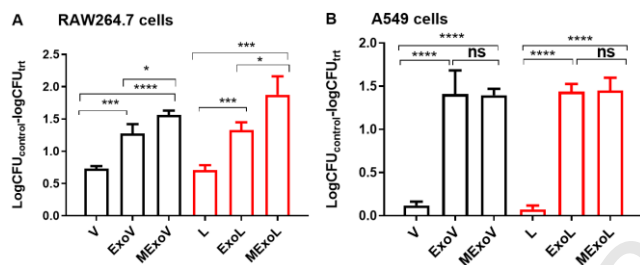


**Figure 8.** Effects of drug loaded unmodified exosomes or modified exosomes on intracellular MRSA in 2 h infected RAW264.7 cells (A) and A549 cells (B). MRSA WHO-2 infected cells were incubated with V, ExoV, MExoV, L, ExoL or MExoL (10 µg/mL, equiv. V; 5 µg/mL, equiv. L) for 24 h. The control group was treated with PBS. The intracellular bacteria were measured as CFU per mg of protein of cells. V, vancomycin; ExoV, vancomycin loaded exosomes; MExoV, vancomycin loaded mannoseylated exosomes; L, lysostaphin; ExoL, lysostaphin loaded exosomes; MExoL, lysostaphin loaded mannoseylated exosomes. Data represent the mean  $\pm$  SD of three independent experiments in triplicate. \*,  $p < 0.05$ ; \*\*,  $p < 0.01$ ; \*\*\*,  $p < 0.001$ ; \*\*\*\*,  $p < 0.0001$ .

### 3.6. Cellular Accumulation of Vancomycin in RAW264.7 Cells

We further determined the cellular accumulation of vancomycin in 4 h for MExoV in MRSA-infected RAW264.7 cells, which were compared with that for ExoV and free V. As shown in **Fig. 7B**, the highest concentration of intracellular vancomycin was observed in macrophages treated with MExoV, followed by ExoV and free V. When macrophages were incubated with MExoV, the intracellular drug accumulation ( $82.68 \pm 3.46$  µg/mg protein of cells) was significantly higher than that treated with ExoV ( $31.57 \pm 1.51$  µg/mg protein of cells). The intracellular accumulation of free vancomycin ( $6.36 \pm 0.88$  µg/mg protein of cells) was approximately twelve times lower than that of MExoV after four hours of incubation. This result showed that MExos could increase intracellular accumulation of vancomycin, which was effectively released into the cells. Similarly, lysostaphin also has good intracellular release (Fig.S14).

### 3.7. In vitro Intracellular Bactericidal Effect of MExoV or MExoL

As MExos enhanced drug delivery into macrophages and MExodrug exhibited good intracellular drug accumulation, we proceeded to investigate their ability to clear intracellular MRSA in 2 h infected RAW264.7 cells or A549 cells by counting CFU of surviving intracellular bacteria. After 24 h of treatment, MExoV and MExoL exhibited significantly better inhibitory effects against intracellular bacteria compared to ExoV and ExoL in MRSA-infected macrophages (**Fig. 8A**), which was not observed in MRSA-infected A549 cells (**Fig. 8B**). Free vancomycin and lysostaphin had no significant inhibitory effect, showing similar CFU as the control that received no treatment. These data demonstrated superior killing of intracellular MRSA by MExodrug, which can be accounted for by its efficient drug delivery to MRSA infected RAW264.7 cells.

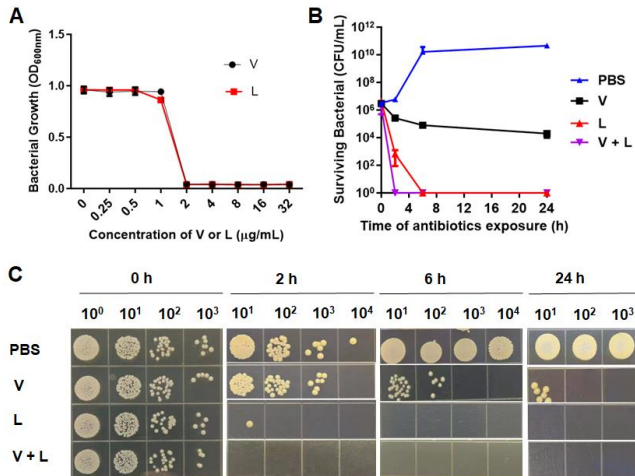


**Figure 9.** (A) MIC determination for V and L on planktonic bacteria MRSA WHO-2 ( $n = 4$ ). (B), (C), Time course of kill for free antibiotics on non-replicating MRSA. The non-replicating bacteria were incubated with V, L or combination of V and L (V = 10 μg/mL; L = 2 μg/mL;  $n = 3$ ) for 24 h. V, vancomycin; L, lysostaphin.

### 3.8. *In vitro* Killing of Intracellular Non-replicating MRSA with Combined MEoV and MEoL

As lysostaphin's antimicrobial activity is independent of the bacterial metabolic state, we speculate that lysostaphin could exhibit potent antibacterial activity against non-replicating MRSA. For planktonic bacteria, lysostaphin and vancomycin showed similar MIC (2 μg/mL) (Fig. 9A). As predicted, lysostaphin could effectively kill non-replicating MRSA in 24 h at the MIC concentration (Fig. 9B and C). However, vancomycin had moderate effect on recovery of persister cells even treatment with five-times MIC concentration (Fig. 9B and C), consistent with the previous report<sup>40</sup>. Interestingly, combination of vancomycin and lysostaphin obviously eliminated the non-replicating MRSA in the culture medium. Lysostaphin could kill not only planktonic bacteria but also quiescent bacteria growing in a biofilm<sup>20,21</sup>. Vancomycin exerts antimicrobial effects when the bacteria are replicating, because of its effect mechanism by primarily inhibiting the biosynthesis of Gram-positive cell walls<sup>43</sup>. The previous study demonstrated that combination of lysostaphin and vancomycin exhibited synergistic antibacterial activity against extracellular *S. aureus* and MRSA<sup>22</sup>. Based on these data, it is speculated that combined MEoV or MEoL could eliminate intracellular non-replicating bacteria.

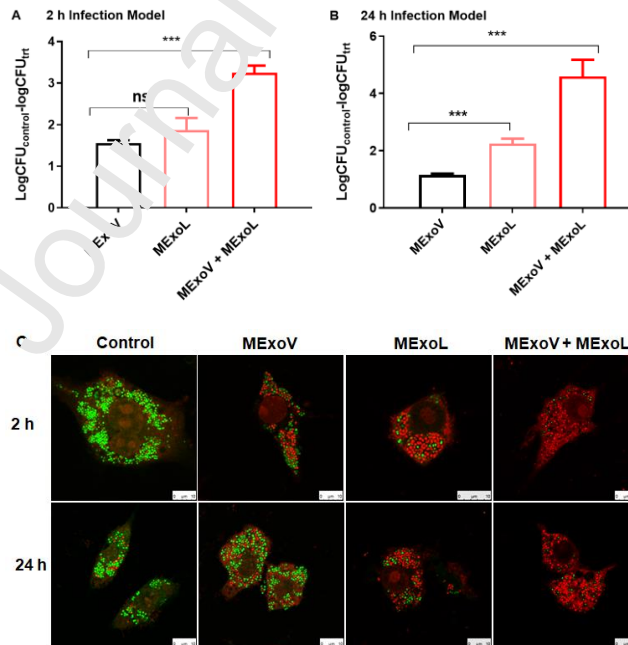


**Figure 10.** Intracellular antimicrobial activity of combined MEoV and MEoL in the 2 h and 24 h infection models. After 2 h (A) or 24 h (B) infection with MRSA, RAW264.7 cells were treated with MEoV, MEoL or combination of MEoV and MEoL for 24 h. The intracellular bacteria were determined as CFU per mg of cell protein after treatment. Data represent the mean  $\pm$  SD of three independent experiments in triplicate. The living (green) and dead (red) intracellular MRSA were also stained with Live/Dead BacLight® kit and observed by confocal microscopy. Scale bars: 10 μm. All treatments were equivalent to 10 μg/mL of V and 5 μg/mL of L. V, vancomycin; L, lysostaphin. \*,  $p < 0.05$ ; \*\*,  $p < 0.01$ ; \*\*\*,  $p < 0.001$ .

It is well documented that after invasion of host cells, *S. aureus* could enter a dormant state to survive within cells, leading to treatment failure<sup>44</sup>. However, at present, it is not clear when bacteria fully enter a dormant state after invasion of host cells, most likely due to technical limitations and the ability of persister cells to revert rapidly in the extracellular milieu. Therefore, to fully explore the intracellular antibacterial effect against non-replicating bacteria *in vitro*, MEoV or MEoL was tested in two kinds of intracellular

infection models, including 2 h infection model and 24 h infection model. As shown in Fig. 10A and B, the intracellular bactericidal effect of MExoV in the 24 h infection model was significantly lower than that of 2 h infection model. It could be speculated that more bacteria go into a dormant state in cells in the 24 h infection model. Interestingly, combination treatment of MExoV and MExoL exhibited significantly better inhibitory capability against intracellular MRSA than that of them alone in both infection models (Fig. 10A and B). Especially, in the 24 h infection model, the CFU of surviving intracellular bacteria treated with combination of MExoV and MExoL was about 3.44 and 2.35 logCFU lower than that of them alone, respectively. CLSM images displayed similar results (Fig. 10C). These results revealed the superior inhibition of intracellular bacterial growth by combination treatment of MExoV and MExoL, which can be accounted for by the different bactericidal mechanisms of vancomycin and lysostaphin.

### 3.9. *In vivo* Antibacterial Effect of MExoV and MExoL

To further explore the antibacterial effect *in vivo*, MExoV or MExoL was tested in abdominally infected mice. As shown in Fig. 11D, combination treatment of MRSA-infected mice with MExoV and MExoL significantly eliminated detectable bacteria in kidneys, whereas the efficacy of free drugs was limited. In the peritoneal fluid, except for the extracellular bacteria (Fig. 11B), MExoV and MExoL exhibited a better inhibitory effect than their free form (Fig. 11A and C). Interestingly, intracellular bacteria were efficiently killed by combination of MExoV and MExoL (Fig. 11C), which is consistent with that observed *in vitro*. These data demonstrated that MEXos encapsulated molecules were able to efficiently inhibit the growth of intracellular bacteria *in vitro* and *in vivo*.

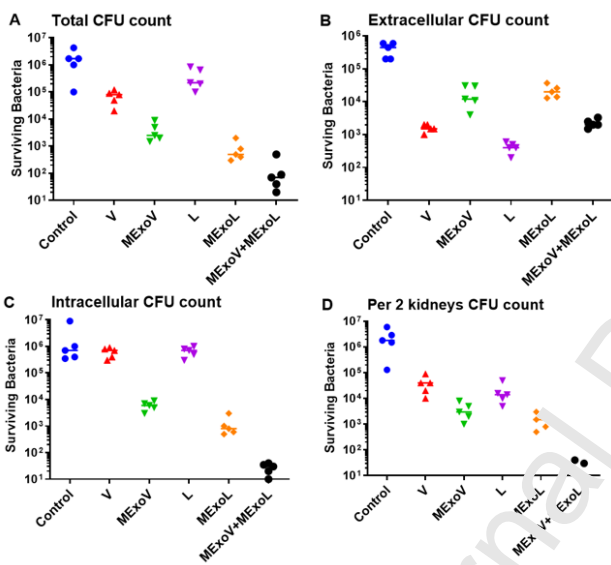


**Figure 11.** Evaluation of antibacterial efficiency of MExoV and MExoL in MRSA infected mice (CFU, mean $\pm$ SD; n = 5). (A-C), MRSA-infected mice were injected intravenously with a single dose of V (20 mg/kg), MExoV (V = 20 mg/kg), L (5 mg/kg), MExoL (L = 5 mg/kg), or combination of MExoV and MExoL (V = 20 mg/kg, L = 5 mg/kg). The control group was injected with PBS. After 24 h treatment, survival of MRSA in the peritoneal fluid was determined. The effect was estimated both in total (A) and when divided into extra- (B) and intracellular (C) fractions. (D) Infected mice were treated with drugs as described above (A-C) by intravenous injection once a day for 3 days. Survival bacteria was tested in per 2 kidneys by the agar plate. V, vancomycin; MExoV, vancomycin loaded mannosylated exosomes; L, lysostaphin; MExoL, lysostaphin loaded mannosylated exosomes.

### 3.10. *In vivo* Toxicity of MEXos and MEXodrug

To evaluate the toxicity of MEXos and MEXodrug *in vivo*, the major organs (heart, liver, spleen, lung, kidney) of the tested mice were collected after three days of treatment with five times of the therapeutic dose and tested by H&E staining. There was no death and loss of weight in all treatment groups. In Fig. 12, the organs of all the treatment groups exhibited normal histomorphology and no significant pathological abnormality. In the meantime, the biocompatibility of MEXos and MEXodrug was also tested *in vitro*, which showed no significant cytotoxicity in cell culture (Fig. S15). These results suggested that MEXos and MEXodrug had good biocompatibility *in vitro* and *in vivo*.

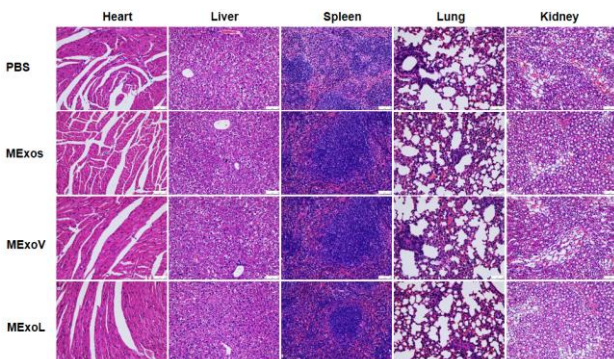


**Figure 12.** Acute toxicity of MEXos, MEXoV and MEXoL to major organs in mice. Mice were treated with MEXos (2.5 mg/kg), MEXoV (V = 100 mg/kg) or MEXoL (L = 25 mg/kg) by intravenous injection once a day for 3 days. The control group was injected with PBS. Various organs from treated or untreated mice were stained with hematoxylin and eosin (H&E). Scale bars: 75  $\mu$ m.

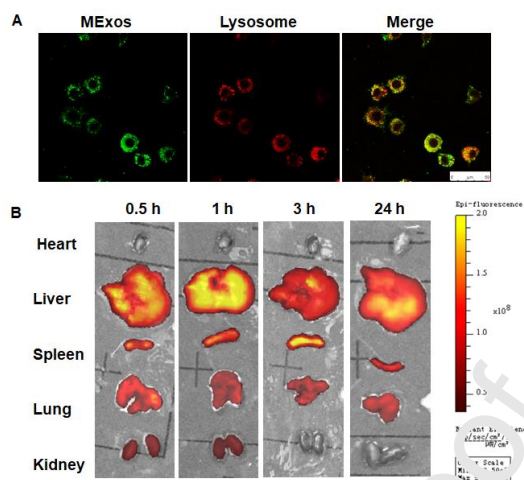


**Figure 13.** (A) Intracellular pathway of MEXos in RAW264.7 cells after 24 h incubation. Scale bars: 50  $\mu$ m. (B) *Ex vivo* imaging of major organs in 24 h post-injection.

### 3.11. Intracellular Localization of MEXos and their Tissue Distribution in Mice

Furthermore, we determined the intracellular localization of MEXos in MRSA infected RAW264.7 cells. Infected cells were incubated with DiO-labeled MEXos for 24 h and the lysosomes were labeled with LysoTracker red. CLSM images suggested that MEXos likely co-localized with the lysosomes (Fig. 13A), which is the shelter for *S. aureus* within cells<sup>7</sup>. Additionally, we assessed the tissue distribution of MEXos *in vivo*. KM mice were injected with DiD-labeled MEXos via tail vein and imaged over time using an IVIS imaging system. As shown in Fig. 13B, strong DiD signals were observed in the liver and spleen in 24 h, followed by lung. Very weak signals were observed in other organs. More importantly, MEXos rapidly accumulated in the liver and spleen at 0.5 h post-injection. It is well known that the liver and spleen are the target organs where infected macrophages are predominantly located<sup>45</sup>. Thus, the mannoseylated exosomes could preferentially deliver the encapsulated antibiotic to macrophages, and transport the antibiotic to the bacterial infection site *in vivo*.

## 4. Conclusions

In summary, we developed a novel nanoparticle platform that employs the mannoseylated exosomes to deliver lysostaphin and vancomycin to bacterial infection sites to eradicate intracellular MRSA. Lysostaphin is targeted against *Staphylococcus* species and showed no toxicity. The combination bactericidal strategy would reduce the dose of vancomycin, and thereby toxicity, as well as resistance. This strategy opens a new avenue in combating invasive bacterial infections of macrophages such as MRSA.

## Supporting Information

For NMR spectra of the synthesized compounds, see Supplementary Figs. 1-13; For detailed experimental procedures, see Supplementary Methods; For intracellular release of lysostaphin in RAW 264.7 cells, see Supplementary Fig. 14; For cytotoxicity of MEXos, MEXoV or MEXoL on RAW 264.7 cells, see Supplementary Fig. 15.

## Author Contributions

X.Y., B. X., H.P., and Y.H. conceived the entire study and designed the experiments; B.X., H.P., B.S. and J. G performed the organic synthesis experiments; X. Y. performed the biological experiments and analyzed the data; G.S. performed the determination of antibiotic concentrations and interpretation of the results; C.W made substantial contributions to the *in vivo* experiments; X.Y. and H.P. wrote the paper; X.Y., B.X., H.P., C. W and Y.H. reviewed the manuscript. All authors discussed and commented on the data in this manuscript.

## Declaration of Competing Interest

The authors declare no competing financial interest.

## Acknowledgments

We thank the National Nature Science Foundation (No. 21572027 and No.81703424 ) and Ministry of Science and Technology (No. 2019ZX09301164) of China, Chongqing Science and Technology Bureau (csts2019jcyj-zdxmX0021). We thank Yanfei Qiu for technical assistance with detecting intracellular bactericidal effect of Exodrug. And we thank Yanfei Qiu, Yongjun Ji, Huan Du and Junhao Zhu for technical assistance with detecting *in vivo* antibacterial effect of MEXodrugs. We also thank Dr. Rongxin Qin (Army Military Medical University, Chongqing, China) for kindly providing the MRSA WHO-2 strain.

## References

1. Patini, R., *et al.* The effect of different antibiotic regimens on bacterial resistance: a systematic review. *Antibiotics* **9**, 22(2020).
2. Harris, A., Pineles, L. & Perencevich, E. Recognising the value of infection prevention and its role in addressing the antimicrobial resistance crisis. *BMJ Qual. Saf.* **26**, 683-686(2017).
3. Tong, S.Y.C., *et al.* *Staphylococcus aureus* infections: epidemiology, pathophysiology, clinical manifestations, and management. *Clin. Microbiol. Rev.* **28**, 603-661(2015).
4. Turner, N.A., *et al.* Methicillin-resistant *Staphylococcus aureus*: an overview of basic and clinical research. *Nat. Rev. Microbiol.* **17**, 203-218(2019).
5. Mège, J.L., Mehraj, V. & Capo, C. Macrophage polarization and bacterial infections. *Curr. Opin. Infect. Dis.* **24**, 230-234(2011).
6. Fraunholz, M. & Sinha, B. Intracellular *Staphylococcus aureus*: live-in and let die. *Front. Cell. Infect. Microbiol.* **2**, 1-10(2012).
7. Carryn, S., *et al.* Intracellular pharmacodynamics of antibiotics. *Infect. Dis. Clin.* **17**, 615-634(2003).
8. Tulkens, P.M. Intracellular distribution and activity of antibiotics. *Eur. J. Clin. Microbiol.* **10**, 100-106(1991).
9. Renard, C., *et al.* Influence of conversion of penicillin G into a basic derivative on its accumulation and subcellular localization in cultured macrophages. *Antimicrob. Agents Ch.* **31**, 410-416(1987).
10. Tulkens, P. & Trouet, A. The uptake and intracellular accumulation of aminoglycoside antibiotics in lysosomes of cultured rat fibroblasts. *Bioche. Pharmacol.* **27**, 415-424(1978).
11. Al-Nawas, B. & Shah, P.M. Intracellular activity of vancomycin and Ly333328, a new semisynthetic glycopeptide, against methicillin-resistant *Staphylococcus aureus*. *Infection* **26**, 165-167(1998).
12. Proctor, R.A., Balwit, J.M. & Vesga, O. Variant subpopulations of *Staphylococcus aureus* as cause of persistent and recurrent infections. *Infect. Agents Dis.* **3**, 302-312(1994).
13. Proctor, R.A., *et al.* Persistent and relapsing infections associated with small-colony variants of *Staphylococcus aureus*. *Clin. Infect. Dis.* **20**, 95-102(1995).
14. Schindler, C.A. & Schuhardt, V. Lysostaphin: a new bacteriolytic agent for the *Staphylococcus*. *Acad. Sci. USA* **51**, 414(1964).
15. Kumar, J.K. Lysostaphin: an antistaphylococcal agent. *Appl. Microbiol. Biot.* **80**, 555-561(2008).
16. Placencia, F.X., Kong, L. & Weisman, L.E. Treatment of methicillin-resistant *Staphylococcus aureus* in neonatal mice: lysostaphin versus vancomycin. *Pediatr. Res.* **65**, 420-424(2009).
17. Kokai-Kun, J.F., *et al.* Lysostaphin cream eradicates *Staphylococcus aureus* nasal colonization in a mouse rat model. *Antimicrob. Agents Ch.* **47**, 1589-1597(2003).
18. Bastos, M.d.C.d.F., Coutinho, B.G. & Coelho, M.L.V. Lysostaphin: a staphylococcal bacteriolytic with potential clinical applications. *Pharmaceuticals* **3**, 1139-1161(2010).
19. Climo, M.W., *et al.* Lysostaphin treatment of experimental methicillin-resistant *Staphylococcus aureus* aortic valve endocarditis. *Antimicrob. Agents Ch.* **42**, 1355-1360(1998).
20. Kokai-Kun, J.F., Chanturiya, T. & Mond, J.J. Lysostaphin eradicates established *Staphylococcus aureus* biofilms in jugular vein catheterized mice. *J. Antimicrob. Chemoth.* **64**, 94-100(2009).
21. Ceotto - Vigoder, H., *et al.* Nisin and lysostaphin activity against preformed biofilm of *Staphylococcus aureus* involved in bovine mastitis. *J. Appl. Microbiol.* **121**, 101-114(2016).
22. Hajjahmadi, F., *et al.* The bactericidal effect of lysostaphin coupled with liposomal vancomycin as a dual combating system applied directly on methicillin-resistant *Staphylococcus aureus* infected skin wounds in mice. *Int. J. Nanomed.* **14**, 5943(2019).
23. Zhang, M., *et al.* Exosome-based nanocarriers as bio-inspired and versatile vehicles for drug delivery: recent advances and challenges. *J. Mater. Chem. B* **7**, 2421-2433(2019).
24. Jiang, L., *et al.* Exosomes: diagnostic biomarkers and therapeutic delivery vehicles for cancer. *Mol. Pharmaceut.* **16**, 3333-3349(2019).
25. Arenaccio, C., *et al.* Exosomes in therapy: engineering, pharmacokinetics and future applications. *Curr. Drug Targets* **20**, 87-95(2019).
26. Alvarez-Erviti, L., *et al.* Delivery of siRNA to the mouse brain by systemic injection of targeted exosomes. *Nat. Biotechnol.* **29**, 341(2011).
27. Antimisiaris, S., Mourtas, S. & Marazioti, A. Exosomes and exosome-inspired vesicles for targeted drug delivery. *Pharmaceutics* **10**, 218(2018).
28. Fan, Z., *et al.* Functionalized DNA enables programming exosomes, vesicles for tumor imaging and therapy. *Small* **15**, 1-11(2019).
29. Dang, X.T. & Zeng, X.R. Targeted therapeutic delivery using engineered exosomes and its applications in cardiovascular diseases. *Gene* **575**, 377-384(2016).
30. Haney, M.J., *et al.* Exosomes as drug delivery vehicles for Parkinson's disease therapy. *J. Control. Release* **207**, 18-30(2015).
31. Yang, X., *et al.* Exosome-encapsulated antibiotic against intracellular infections of methicillin-resistant *Staphylococcus aureus*. *Int. J. Nanomed.* **13**, 8095(2018).
32. Aryani, A. & Denecke, B. Exosomes as a nanodelivery system: a key to the future of neuromedicine? *Mol. Neurobiol.* **53**, 818-834(2016).
33. Turturici, G., *et al.* Extracellular membrane vesicles as a mechanism of cell-to-cell communication: advantages and disadvantages. *Am. J. Physiol-Cell Ph.* **306**, C621-C633(2014).
34. More, S.S. & Vince, R. Inhibition of glyoxalase I: the first low-nanomolar tight-binding inhibitors. *J. Med. Chem.* **52**, 4650-4656(2009).
35. Bernardes, G.J., *et al.* Site-selective traceless staudinger ligation for glycoprotein synthesis reveals scope and limitations. *Chem. Bio. Chem.* **12**, 1383-1386(2011).
36. Wang, M., *et al.* Integrating protein engineering and bioorthogonal click conjugation for extracellular vesicle modulation and intracellular delivery. *PLoS One* **10**, 1-12(2015).
37. Tian, Y., *et al.* A doxorubicin delivery platform using engineered natural membrane vesicle exosomes for targeted tumor therapy. *Biomaterials* **35**, 2383-2390(2014).
38. Yang, X., *et al.* Anti-lung cancer activity and inhibitory mechanisms of a novel Calothrix A derivative. *Life Sci.* **219**, 20-30(2019).
39. Yuan, K., *et al.* Determination of vancomycin in plasma by RP-HPLC. *J. Anhui Med. Pharmaceut.* **14**, 163-165(2010).
40. Lehar, S.M., *et al.* Novel antibody-antibiotic conjugate eliminates intracellular *S. aureus*. *Nature* **527**, 323(2015).
41. Lin, Z., *et al.* Total synthesis and antimicrobial evaluation of natural albomycins against clinical pathogens. *Nat. Commun.* **9**, 1-8(2018).
42. Sandberg, A., *et al.* Intra- and extracellular activities of dicloxacillin and linezolid against a clinical *Staphylococcus aureus* strain with a small-colony-variant phenotype in an *in vitro* model of THP-1 macrophages and an *in vivo* mouse peritonitis model. *Antimicrob. Agents Ch.* **55**, 1443-1452(2011).
43. Levine, D.P. Vancomycin: a history. *Clin. Infect. Dis.* **42**, S5-S12(2006).
44. Sendi, P. & Proctor, R.A. *Staphylococcus aureus* as an intracellular pathogen: the role of small colony variants. *Trends Microbiol.* **17**, 54-58(2009).
45. Pei, Y., *et al.* Particle engineering for intracellular delivery of vancomycin to methicillin-resistant *Staphylococcus aureus* (MRSA)-infected macrophages. *J. Control. Release* **267**, 133-143(2017).

**Highlights**

- ▶ Mannosylated exosomes with the capabilities of macrophage cell-targeting were developed using the metabolic labeling and click chemistry.
- ▶ This mannosylated exosome could enhance the delivery of antibiotics to intracellular pathogens.
- ▶ Combination of vancomycin and lysostaphin loaded exosomes displayed pronounced eradication of intracellular quiescent MRSA.
- ▶ These antibiotics loaded exosomes showed no toxicity.
- ▶ The exosomes encapsulated antibiotics will reduced the dose of vancomycin, followed by decreased toxicity and resistance.

**Author Contributions**

X.Y., B.X., H.P. and Y.H. conceived the entire study and designed the experiments; B.X., H.P., B.S. and J. G performed the organic synthesis experiments; X. Y. performed the biological experiments and analyzed the data; G.S. performed the determination of antibiotic concentrations and interpretation of the results; C.W made substantial contributions to the *in vivo* experiments; X.Y. and H.P. wrote the paper; X.Y., B.X., H.P., C. W and Y.H. reviewed the manuscript. All authors discussed and commented on the data in this manuscript.

Journal Pre-proof